Electronic Supplementary Information (ESI)

Copper Dendrites Stabilized $NiFe(OH)_x$ Electrocatalysts for Durable Alkaline Hydrogen Evolution over 1000 h

Guangming Shang,[a] Yu Liu,[a] Yajiao Li,[a] Wei Qiao,*[a] Chao Wang,[a] Yaru Li,[bc] Dongsheng Zhang,[a] Foteini Sapountzi,[d] Yongwang Li,[bc] Hans Niemantsverdriet,[bd] Mark H Rümmeli,*[a] and Ren Su*[ab]

[a] *Soochow Institute for Energy and Materials Innovations (SIEMIS), Soochow University, Suzhou, 215006, China.*
[b] *SynCat@Beijing, Synfuels China Technology Co. Ltd., Leyuan South Street II, No.1, Yanqi Economic Development Zone C#, Huairou District, Beijing, 101407, China.*
[c] *State Key Laboratory of Coal Conversion, Institute of Coal Chemistry, Taiyuan, 030001, China.*
[d] *SynCat@DIFFER, Syngaschem BV, 6336 HH Eindhoven, The Netherlands.*
Email: mhr1@suda.edu.cn; suren@suda.edu.cn

Table of Contents

Experimental Procedures

Raw Materials: The following commercial precursors were used: $Cu(NO_3)_2{\cdot}3H_2O$, Urea, $NiSO_4{\cdot}6H_2O$, KOH, (Shanghai Aladdin Biochemical Technology Co., Ltd.), $Fe(NO_3)_3{\cdot}9H_2O$, Na_2SO_4, C_2H_5OH (Saen Chemical Technology Co., Ltd.), HCl aqueous solution (1 M), Nafion solution, Commercial Pt/C (20 wt.%) (Johnson Matthey Fuel Cells), Nickel sponge (thickness: 1.0 mm, density: 0.23 $g{\cdot}cm^{-3}$) was purchased from Jiangsu AKX Materials Technology Co. Ltd. Carbon paper (thickness: 0.19 mm, density: 0.44 $g{\cdot}cm^{-3}$) was purchased from Toray. All the chemicals were purchased and used without further purification.

Synthesis of $Ni(OH)_x$ electrodes. The $Ni(OH)_x$ electrodes were synthesized using an electrodeposition method. Nickel sponge was used as a substrate for the electrodeposition. Before electrodeposition, the nickel sponge was ultrasonically washed with 1 M HCl, ethanol and DI water for 30 min, respectively. The deposition electrolytes solution was obtained by dissolving 0.40 g $NiSO_4{\cdot}6H_2O$ (50 mM) and 0.85 g Na_2SO_4 (200 mM) in DI water to reach a final volume of 30 mL and purged with Ar for 30 min before electrodeposition. Electrodeposition was performed using a standard three-electrode system. Nickel sponge (1×1 cm^2), nickel sheets (1×1 cm^2), Ag|AgCl were used as working electrode (WE), counter electrode (CE) and reference electrode (RE), respectively. The applied potential was -1.0 V *vs.* Ag|AgCl for 150 s at room temperature. The resulting samples were washed with DI water and dried in air.

Pt/C electrode preparation. The Pt/C electrode was prepared as follows: 5.0 mg 20% Pt/C powder was dispersed in 980 μL water/ethanol (v/v=1:1) mixed solvent along with 20 μL 5 wt% of Nafion solution and sonicated for 30 min to form a homogeneous solution. Then 200 μL of the catalyst ink was loaded on carbon paper electrode (1×1 cm^2) and dried in air at room temperature. The mass loading of Pt/C was 1.0 mg cm^{-2}.

Material Characterizations.

Powder X-ray diffraction (PXRD). The XRD patterns of the samples were measured using a Bruker AXS D8 Advance diffractometer with Cu Kα source. (40kV, 40mA).

Scanning electron microscope. The morphology of samples was investigated by field emission scanning microscopy (FEI-SEM, Scios – Thermo Fisher).

Auger Electron Spectroscopy (AES) analysis. AES measurements were performed using a PHI 710 system, using a beam energy of 10 kV, with 10 nA beam current.

Cs-Transmission electron microscope. The morphology of samples was obtained by using a Cs-transmission electron microscope (TEM, FEI Titan Themis Cubed G2 300). The samples were dispersed in ethanol and dropped on the Mo grid for analysis.

X-ray photoelectron spectroscopy. The chemical composition and oxidation state of the elements on the catalyst surface were characterized by an X-ray photoelectron spectrometer that is equipped with an Al Kα X-ray source (XPS, Escalab 250Xi, Thermo Fisher, USA). Survey scans were measured from 1200 to -10 eV using a pass energy of 160 eV with a step size of 1 eV and a dwell time of 0.1 s. The high-resolution spectra were collected in the desired energy regions using pass energy of 40 eV with a step size of 0.1 eV and a dwell time of 0.5 s. All binding energies were calibrated using the peak of adventitious carbon at 284.6 eV.

***In Situ* Raman Spectroscopy.** *In situ* Raman measurements were carried out with the samples in a tailor-made cell. Raman spectra of the catalyst, Pt wire, and Ag/AgCl, used as a working, counter, and reference electrode, respectively, were collected using a Horiba Jobin Yvon HR Evolution spectrometer.

Electrochemical Measurements. Electrochemical measurements were performed in a three-electrode cell using a potentiostat (PGU Touch IPS Electroniklabor, Germany). All measurements were made in 1 M KOH electrolyte purged with Ar gas. Hg|HgO (RE) and graphite sheet (CE) were used. The hydrogen evolution reaction (HER) performance was evaluated in the range of 0.424 V to −0.276 V *vs.* RHE at a scan rate of 5 mV s^{-1}.

The long-term water electrolysis test of Cu/NiFe(OH)$_x$ were conducted in a two-electrode system using a LANHE CT2001A (Wuhan Land Electronics CO. Ltd). The NiFe layered double hydroxide (NiFe-LDH) was used as the anode. Chronoamperometric measurement were performed by applying a constant potential to check the stability. The test was carried out in two stages. In the first stage, the stability was tested at 10 mA cm^{-2} with an applied voltage of 1.51 V. In the second stage, the electrolyzer was first operated at 50 mA cm^{-2} for 24 h with an applied voltage of 1.92 V, then the voltage was adjusted to 1.51 V and operated at 10 mA cm^{-2} for 48 h, this cycle was repeated five times. Stirring was applied during the test with a rotational speed of 500 rpm. The electrolyte (1 M KOH) was changed every 24 h.

The series resistance (Rs) obtained from EIS measurements were used to correct the polarization measurement with equation: $E_{Corrected} = E_{Uncorrected} - iRs$.

Supplementary Notes

Note 1. Synthesis of Cu/NiFe(OH)$_x$ electrode: The Cu/NiFe(OH)$_x$ electrode was synthesized *via* a classical hydrothermal process. Firstly, commercial nickel sponge (NS) with an area of 2×4 cm^2 was washed with 1 M HCl, ethanol and deionized (DI) water for 30 minutes, respectively. The cleaned NS was placed in a 100 mL Teflon-lined autoclave. Then, $Cu(NO_3)_2{\cdot}3H_2O$ (15 mM), $Fe(NO_3)_3{\cdot}9H_2O$ (5 mM) and urea (200 mM) were dissolved in 50 mL DI water and transferred to the autoclave. The autoclave was sealed and maintained 120 °C for 12 h and cooled to room temperature. Finally, the resulting sample was washed by DI water, and finally dried in a vacuum oven at 60 °C for 10 h to yield the electrocatalyst.

Note 2. Calculation of dissolved metal: The loading of the metals was determined using inductively coupled plasma-atomic emission spectroscopy (ICP-AES) analysis. The dissolved metal values could be calculated by the following equation:

$$\text{Dissolved metal} = M/T * 100\%$$

where M and T represent the metal dissolved during the reaction and the total amount of metal in one electrode (1×1 cm^2), respectively. An ICP-AES test was performed on a piece of fresh Cu/NiFe(OH)$_x$ electrode (1×1 cm^2) and the results showed that the total amounts of metal in one electrode are estimated to be 113.1 ug (Cu), 29.1 ug (Fe), respectively. The dissolved metals are estimated to be 16% (Cu), 0% (Ni), and 0% (Fe), respectively.

Supplementary Figures

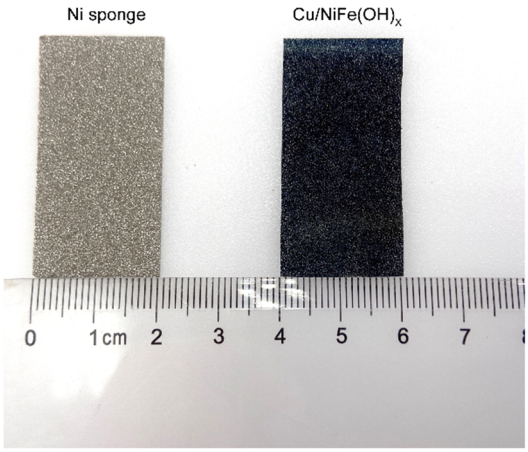

Figure S1. Photographs of Ni sponge and Cu/NiFe(OH)$_x$ deposited on Ni sponge.

The catalyst is uniformly deposited on the Ni sponge substrate.

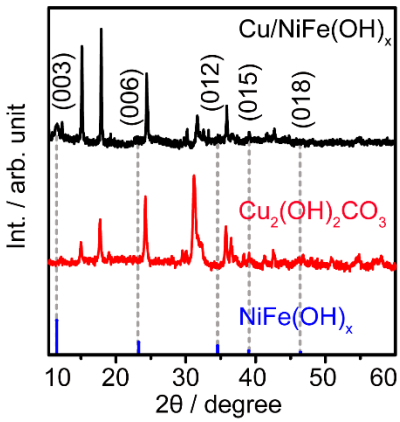

Figure S2. XRD pattern of Cu/NiFe(OH)$_x$.

The diffraction peaks located at 11.5°, 23.2° and 39.0° in XRD pattern are assigned to NiFe(OH)$_x$ (JCPDS Card No. 51-0463), while the peaks located at 14.7°, 17.5°, 24.2° and 35.9° are assigned to $Cu_2(OH)_2CO_3$ (JCPDS Card No. 76-0660).

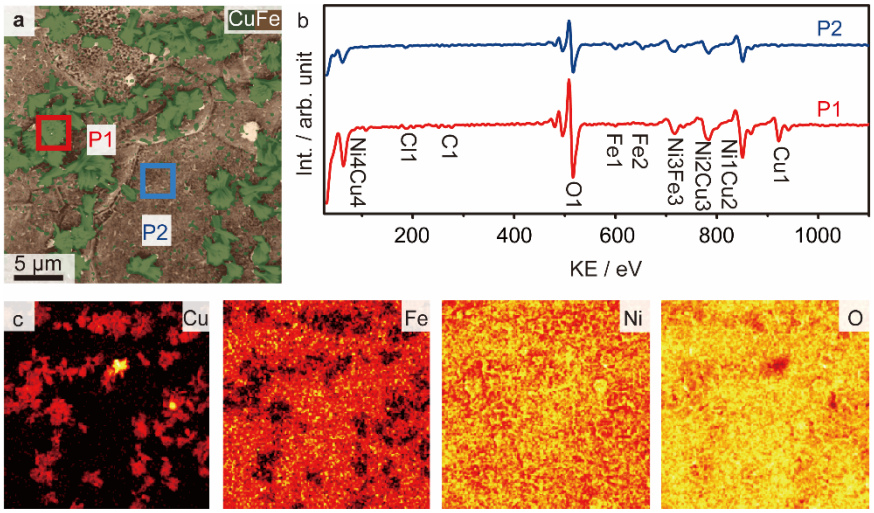

Figure S3. (a) Auger SEM image and (b) survey spectra collected from two regions of Cu/NiFe(OH)$_x$. (c) Auger element mapping of Cu, Fe, Ni, O.

Cu is located in the dendrites, for example marked as region P1 (red square). Fe is mainly located in regions with less Cu (P2, blue square), but can be also found in Cu-rich region (P1). Ni and O are uniformly distributed.

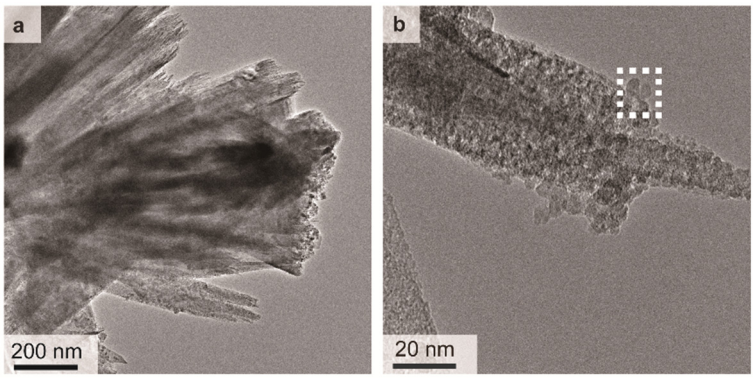

Figure S4. (a) and (b) TEM imaging of the Cu/NiFe(OH)$_x$ dendrites from the Ni sponge by sonication.

On the edge of the malachite dendrite reveals a roughened surface that is homogeneously covered with nanocrystals.

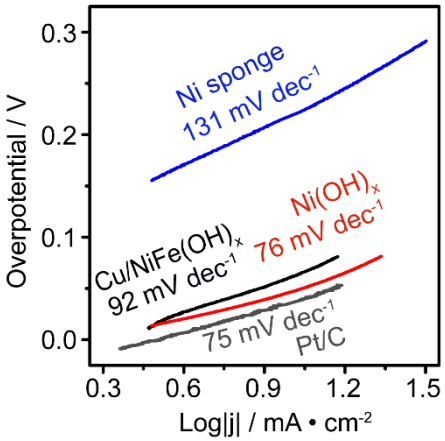

Figure S5. Tafel plots of Cu/NiFe(OH)$_x$, Ni(OH)$_x$, Pt/C and Ni sponge in 1 M KOH.

The Tafel slopes for Pt/C, Ni(OH)$_x$, and Cu/NiFe(OH)$_x$ are 75, 76, and 92 mV·dec^{-1}, respectively. The slightly increased Tafel slope of the Cu/NiFe(OH)x could be possibly related to changes in the kinetics of the steps, either a slightly slower first step (*i.e.* Volmer) or a faster second step (*i.e.* Heyrovsky or Tafel).

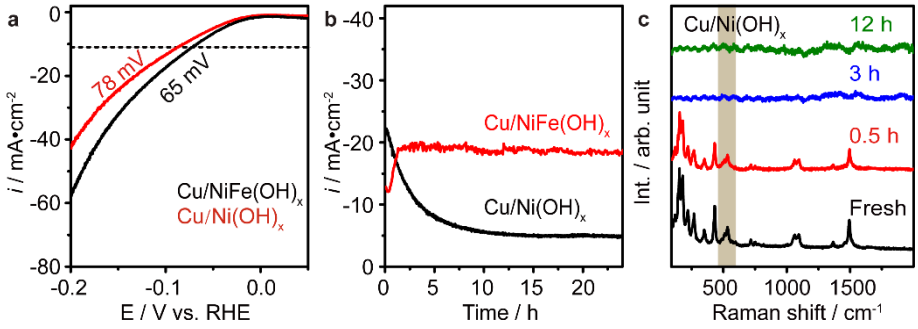

Figure S6. (a) Polarization curves of Cu/NiFe(OH)$_x$, and Cu/Ni(OH)$_x$ electrode for HER. (b) Stability of the Cu/Ni(OH)$_x$ for HER half reaction. (c) Raman spectroscopy of Cu/Ni(OH)$_x$ at different reaction times during HER process.

The electrochemical HER performance of Cu/Ni(OH)$_x$ and Cu/NiFe(OH)$_x$ was studied under identical reaction conditions. While the catalytic activity of Cu/Ni(OH)$_x$ ($\eta_{10\,mA}$ = 78 mV) is close to that of Cu/NiFe(OH)$_x$ ($\eta_{10\,mA}$ = 65 mV, Fig. S6a), the activity of Cu/Ni(OH)$_x$ decays significantly within 10 hours (Fig. S6b). Raman analysis of the Cu/Ni(OH)$_x$ reveals that the Ni(OH)$_x$ nanocrystals gradually disappeared upon increasing the reaction time (Fig. S6c), indicating that Fe also plays an important role in stabilizing the active species of Ni(OH)$_x$. A possible mechanism is that Fe^{3+} may serve as an electron transfer mediator to Cu, thus avoiding the reduction of Ni(OH)$_x$.

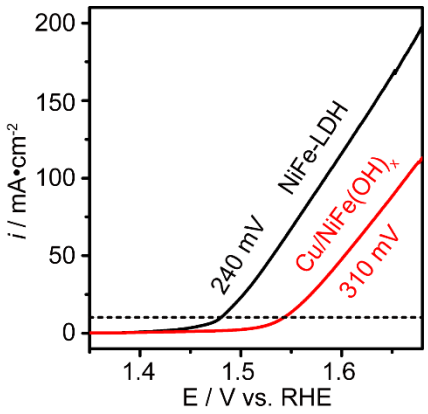

Figure S7. Polarization curves of Cu/NiFe(OH)$_x$ and NiFe-LDH electrode for OER.

The overpotentials of Cu/NiFe(OH)$_x$ and NiFe-LDH electrode for OER are 310 and 240 mV at a current density of 10 mA·cm^{-2}, respectively, indicating that NiFe-LDH is a better candidate for assembling a water electrolyzer.

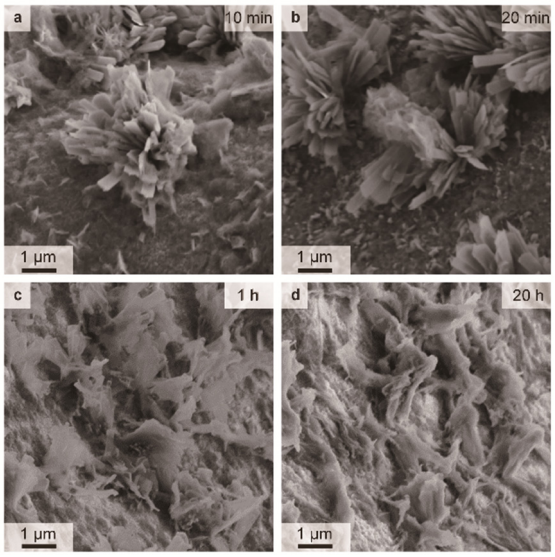

Figure S8. SEM images of the spent Cu/NiFe(OH)$_x$ electrode for HER after different reaction times.

Once the Cu dendrites are completely reduced into metallic Cu during HER (~ 1 h), the morphology of the spent Cu/NiFe(OH)$_x$ remains unchanged for prolonged reaction times.

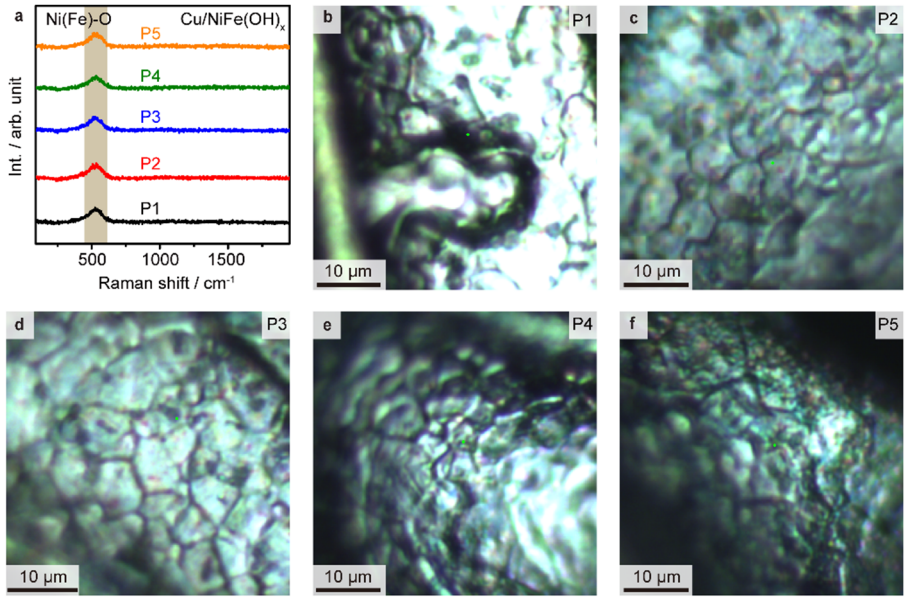

Figure S9. Raman spectroscopy of Cu/NiFe(OH)$_x$ at random positions after 10 minutes of reaction.

The Cu/NiFe(OH)$_x$ electrocatalyst shows a homogeneous surface after 10 min of HER reaction according to Raman analysis of five random positions of the spent catalyst.

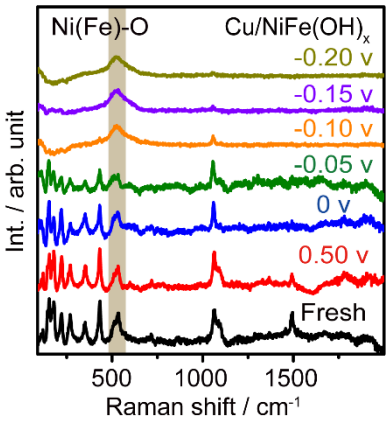

Figure S10. *in-situ* electrochemical Raman spectroscopy of Cu/NiFe(OH)$_x$ recorded during HER half reaction in 1 M KOH at various bias vs. RHE.

The diminishing of malachite polycrystalline starts at a bias of -0.05 V vs. RHE and completes at −0.15 V vs RHE, as indicated by the reduction of characteristic peaks (< 500 cm^{-1} and 1090 cm^{-1}). Meanwhile, the vibrational peak of Ni(Fe)-O at 530 cm^{-1} remains almost identical at all bias, confirming that NiFe(OH)$_x$ is stable within the operation window.

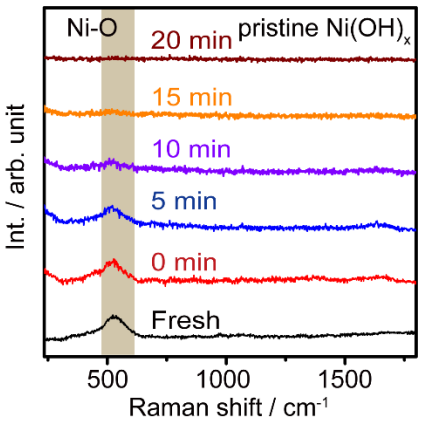

Figure S11. *in-situ* electrochemical Raman spectroscopy of $Ni(OH)_x$ recorded during HER half reaction in 1 M KOH at a current density of 10 $mA \cdot cm^{-2}$.

The peak at 530 cm^{-1} of the pristine $Ni(OH)_x$ gradually disappears over a reaction time of 10 min, implying a compositional or structural change.

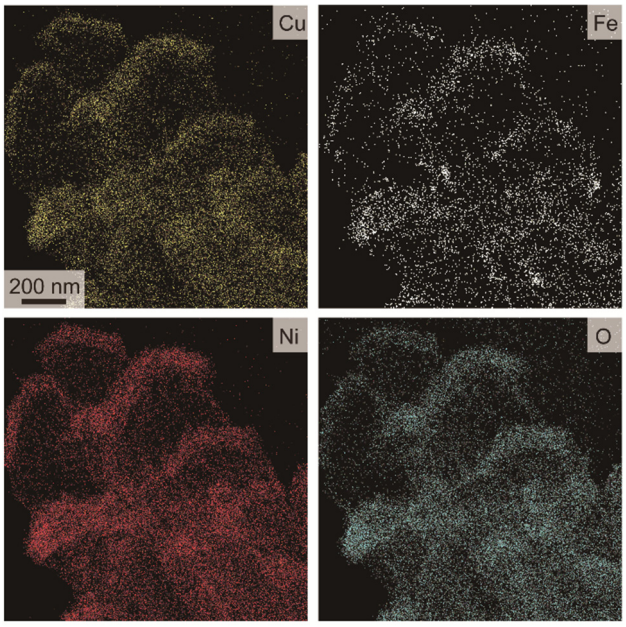

Figure S12. TEM mapping of the Cu/$NiFe(OH)_x$ electrode after electrolysis for 3 h.

Cu, Fe, Ni, and O are homogeneously distributed within the flakes, indicating that the $NiFe(OH)_x$ crystals from the fresh catalyst have migrated from the Ni sponge and covered the Cu flakes.

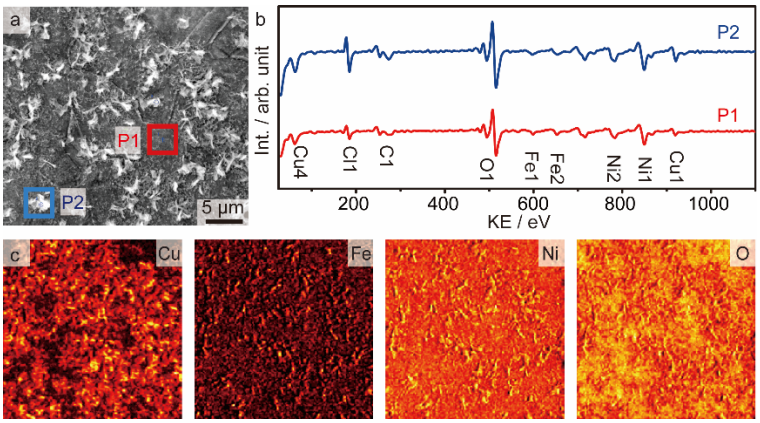

Figure S13. (a) Auger SEM image of the spent Cu/NiFe(OH)$_x$ electrode. (b) Auger survey spectra collected from two regions of Cu/NiFe(OH)x after HER (3 h). (c) Auger element mapping of Cu, Fe, Ni, O."

The bulk Cu dendrites have disappeared after HER reaction. Ni, Fe, O are uniformly distributed.

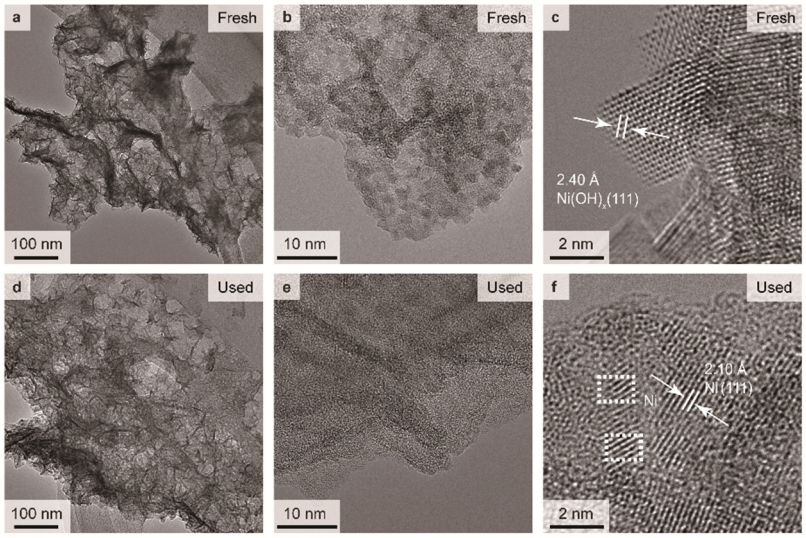

Figure S14. *Ex situ* TEM of pristine Ni(OH)$_x$ (a)-(c) Fresh Ni(OH)$_x$ prior to HER reaction. (d)-(f) TEM images of spent Ni(OH)$_x$ after HER for 3 h.

Nanocrystalline Ni(OH)$_x$ with an interplanar spacing of 2.40 Å is homogeneously dispersed within the freshly prepared pristine Ni(OH)$_x$ electrode. A significant decrease of the crystallinity accompanied with a reduction of the lattice spacing (2.10 Å) is observed for the spent Ni(OH)$_x$, indicating the partial reduction of Ni(OH)$_x$ into metallic Ni.

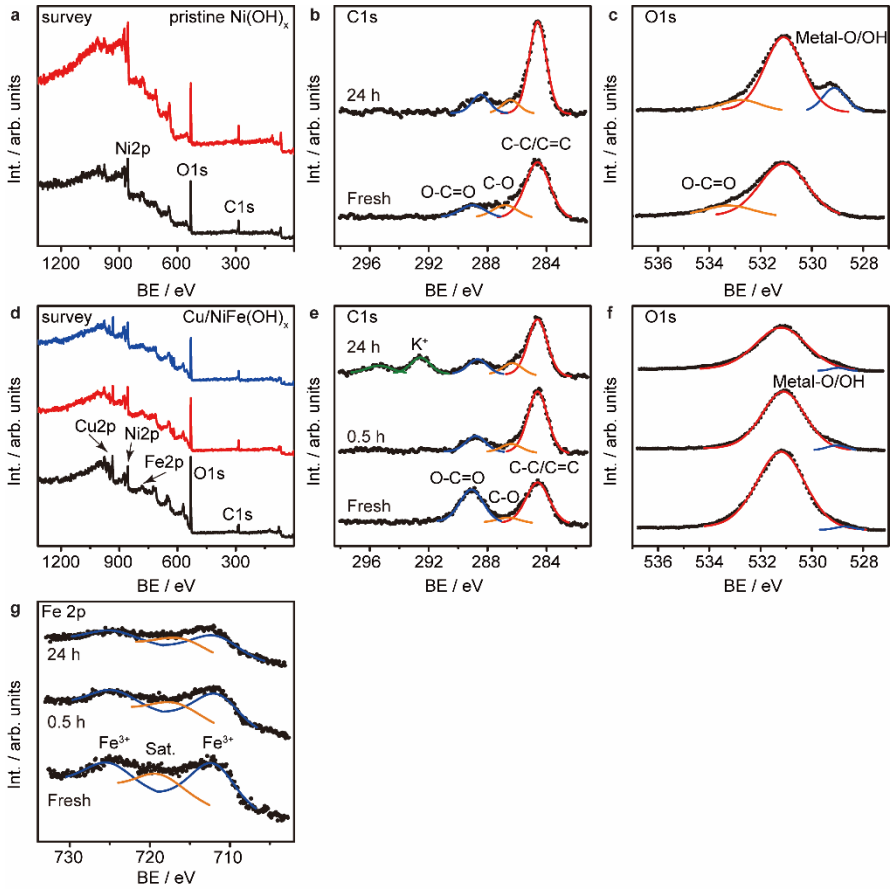

Figure S15. XPS spectrum of the $Ni(OH)_x$ (a)-(c) and $Cu/NiFe(OH)_x$ (d)-(g).

The XPS survey spectra of the pristine $Cu/NiFe(OH)_x$ show the existence of C, O, Cu, Fe and Ni. The apparence of K in the spent catalyst (24 h) is due to KOH in the electrolyte. No change of C1s and O1s is observed after HER. The XPS survey spectra of the pristine $Ni(OH)_x$ show C, O and Ni. An additional O1s peak is observed for the spent catalyst, which is due to the partial reduction of $Ni(OH)_x$.

Since the preparation of Cu/NiFe(OH)x in our work is more close to the synthesis of pristine $NiFe(OH)_x$ and Cu is in the form of malachite, we consider that the majority of Ni and Fe to be Ni^{2+} and Fe^{3+} species, respectively. This agrees well with previous published relevant works.[27, 28]

Supplementary Tables

Table S1. Comparison of voltage and durability of Cu/NiFe(OH)$_x$ electrocatalysts in alkaline medium for various electrocatalysts in the literature.

Catalysts	Voltage (V)	Time (h)	Refs. (1-15)
Cu/NiFe(OH)$_x$	1.51	1000	This work
Co-Ni-B/NF	1.72	12	1
$NiCo_2O_4$	1.65	36	2
NiO NRs-m-Ov	1.64	20	3
Ni/Mo_2C-NCNFs	1.64	100	4
NiSe/NF	1.63	20	5
Ni/Ni_8P_3	1.61	24	6
Ni/Ni(OH)$_2$	1.60	20	7
Ni NP|Ni–N–C	1.58	10	8
MoS_2/Ni_3S_2	1.56	10	9
$NiCo_2S_4$	1.58	72	10
NiFe LDH@NiCoP/NF	1.57	100	11
Cu@NiFe LDH	1.54	48	12
MoS_2-Ni_3S_2 HNRs/NF	1.50	48	13
Ni_2P/Ni/NF	1.49	40	14
$MoNi_4$	1.47	10	15

Table S2. Comparison of HER performance in alkaline media for various electrocatalysts.

Catalysts	η10 (mV)	Tafel slope (mV dec^{-1})	Refs. (16-26)
$Cu/NiFe(OH)_x$	65	92	This work
Ni_3N_{1-x}/NF	55	54	16
NiCoP	58	57	17
NiP_2-650(c/m)	134	67	18
NiCu@C	94	94.5	19
Cu/Ni_3S_2	128	76.2	20
$Fe(OH)_x$@Cu-MOF	112	76	21
$Ni/Ni(OH)_2$	77	53	22
NiO/Ni-CNT	80	82	23
P-MoP/Mo_2N	89	78	24
NiO NRs	110	100	25
$Ni_{1-x}CoxSe_2$	85	52	26

Supplementary References

1 N. Xu, G. Cao, Z. Chen, Q. Kang, H. Dai and P. Wang, *J. Mater. Chem. A*, 2017, **5,** 12379-12384.

2 X. Gao, H. Zhang, Q. Li, X. Yu, Z. Hong, X. Zhang, C. Liang and Z. Lin, *Angew. Chem. Int. Ed.*, 2016, **55,** 6290-6294.

3 T. Zhang, M.-Y. Wu, D.-Y. Yan, J. Mao, H. Liu, W.-B. Hu, X.-W. Du, T Ling and S.-Z Qiao, *Nano Energy*, 2018, **43,** 103-109.

4 M. Li, Y. Zhu, H. Wang, C. Wang, N. Pinna and X Lu, *Adv. Energy Mater.*, 2019, **9**, 1803185.

5 C. Tang, N. Cheng, Z. Pu, W. Xing and X Sun, *Angew. Chem. Int. Ed.*, 2015, **54***,* 9351-9355.

6 G. F. Chen, T. Y. Ma, Z. Q. Liu, N. Li, Y. Z. Su, K. Davey and S. Z Qiao, *Adv. Funct. Mater.*, 2016, **26***,* 3314-3323.

7 L. Dai, Z. N. Chen, L. Li, P. Yin, Z. Liu and H. Zhang, *Adv. Mater.*, 2020, **32***,* 1906915.

8 C. Lei, Y. Wang, Y. Hou, P. Liu, J. Yang, T. Zhang, X. Zhuang, M. Chen, B. Yang, L. Lei, C. Yuan, M. Qiu and X. Feng, *Energy Environ. Sci.*, 2019, **12**, 149-156.

9 J. Zhang, T. Wang, D. Pohl, B. Rellinghaus, R. Dong, S. Liu, X. Zhuang and X Feng, *Angew. Chem. Int. Ed.*, 2016, **55**, 6702-6707.

10 Z. Kang, H. Guo, J. Wu, X. Sun, Z. Zhang, Q. Liao, S. Zhang, H. Si, P. Wu, L. Wang and Y. Zhang, *Adv. Funct. Mater.*, 2019, **29**, 1807031.

11 H. Zhang, X. Li, A. Hähnel, V. Naumann, C. Lin, S. Azimi, S. L. Schweizer, A. W. Maijenburg and R. B. Wehrspohn, *Adv. Funct. Mater.*, 2018, **28**, 1706847.

12 L. Yu, H. Zhou, J. Sun, F. Qin, F. Yu, J. Bao, Y. Yu, S. Chen and Z. Ren, *Energy Environ. Sci.*, 2017, **10**, 1820-1827.

13 Y. Yang, K. Zhang, H. Lin, X. Li, H. C. Chan, L. Yang and Q. Gao, *ACS Catal.*, 2017, **7**, 2357-2366.

14 B. You, N. Jiang, M. Sheng, M. W. Bhushan and Y. Sun, *ACS Catal.*, 2015, **6**, 714-721.

15 J. Zhang, T. Wang, P. Liu, Z. Liao, S. Liu, X. Zhuang, M. Chen, E. Zschech and X. Feng, *Nat. Commun.,* 2017, **8**, 15437.

16 B. Liu, B. He, H. Q. Peng, Y. Zhao, J. Cheng, J. Xia, J. Shen, T. W. Ng, X. Meng, C. S. Lee and W. Zhang, *Adv. Sci.*, 2018, **5**, 1800406.

17 Z. Fang, L. Peng, Y. Qian, X. Zhang, Y. Xie, J. J. Cha and G. Yu, *J. Am. Chem. Soc.*, 2018, **140**, 5241-5247.

18 Q. Fu, X. Wang, J. Han, J. Zhong, T. Zhang, T. Yao, C. Xu, T. Gao, S. Xi, C. Liang, L. Xu, P. Xu and B. Song, *Angew. Chem. Int. Ed.*, 2021, **60**, 259-267.

19 Y. Shen, Y. Zhou, D. Wang, X. Wu, J. Li and J. Xi, *Adv. Energy Mater.*, 2018, **8**, 1701759.

20 J. X. Feng, J. Q. Wu, Y. X. Tong and G. R. Li, *J. Am. Chem. Soc.*, 2018, **140**, 610-617.

21 W. Cheng, *Sci. Adv.*, 2021, **7**, eabg2580.

22 L. Dai, Z. N. Chen, L. Li, P. Yin, Z. Liu and H. Zhang, *Adv. Mater.*, 2020, **32**, 1906915.

23 M. Gong, W. Zhou, M. C. Tsai, J. Zhou, M. Guan, M. C. Lin, B. Zhang, Y. Hu, D. Y. Wang, J. Yang, S. J. Pennycook, B. J. Hwang and H. Dai, *Nat. Commun.*, 2014, **5**, 4695.

24 Y. Gu, A. Wu, Y. Jiao, H. Zheng, X. Wang, Y. Xie, L. Wang, C. Tian and H. Fu, *Angew. Chem. Int. Ed.*, 2021, **60**, 6673-6681.

25 T. Zhang, M.-Y. Wu, D.-Y. Yan, J. Mao, H. Liu, W.-B. Hu, X.-W. Du, T. Ling and S.-Z. Qiao, *Nano Energy*, 2018, **43**, 103-109.

26 B. Liu, Y. F. Zhao, H. Q. Peng, Z. Y. Zhang, C. K. Sit, M. F. Yuen, T. R. Zhang, C. S. Lee and W. J. Zhang, *Adv. Mater.*, 2017, **29**, 1606521.

27 Z. Lu, W. Xu, W. Zhu, Q. Yang, X. Lei, J. Liu, Y. Li, X. Sun and X. Duan, *Chem. Commun.*, 2014, **50**, 6479-6482.

28 M. Gong, Y. Li, H. Wang, Y. Liang, J. Z. Wu, J. Zhou, J. Wang, T. Regier, F. Wei and H. Dai, *J. Am. Chem. Soc.*, 2013, **135**, 8452-8455.